EKSPLOATACJA I NIEZAWODNOŚĆ MAINTENANCE AND RELIABILITY

Eksploatacja i Niezawodnosc – Maintenance and Reliability

Volume 24 (2022), Issue 2

journal homepage: http://www.ein.org.pl

Article citation info:
Wang Y, Xie MJ, Su C. Dynamic reliability evaluation of buried corroded pipeline under rockfall impact. Eksploatacja i Niezawodnosc – Maintenance and Reliability 2022; 24 (2): 275–288, http://doi.org/10.17531/ein.2022.2.9.

Indexed by: Web of Science Group

Dynamic reliability evaluation of buried corroded pipeline under rockfall impact

Yifei Wang[a,#], Mingjiang Xie[a,#], Chun Su[a, b,*]

[a] Southeast University, School of Mechanical Engineering, Nanjing 211189, China
[b] Hunan University of Science and Technology, Hunan Provincial Key Lab of Health Maintenance for Mechanical Equipment, Xiangtan 411201, Hunan, China

Highlights

- The relationship between pipeline stress and rockfall parameters is quantified.
- Dynamic response of buried corroded pipeline under load impact is analyzed.
- The corroded pipeline's dynamic reliability under rockfall impact is evaluated.

Abstract

Load impact, such as the rockfall, may bring significant threats to the integrity management of pipeline. This study is intended to evaluate the reliability of buried pipeline under rockfall impact, and so as to reduce the possible failure and unnecessary downtime. Firstly, the dynamic response of the buried pipeline under load is analyzed by Euler Bernoulli foundation beam. After that, the process of rockfall impact on buried corroded pipeline is simulated with nonlinear finite element method. Furthermore, the influence of rockfall's parameters (including rockfall mass, impact velocity, impact position, etc.) on the pipeline's equivalent stress is quantitatively analyzed. Eventually, a time-varying reliability model is established to calculate the failure probability. The results indicate that the mass and velocity of the rockfall have obvious influence on the pipeline's failure probability, and the change of impact's position has small influence. The proposed method can provide a theoretical reference for the design and maintenance of buried pipeline.

Keywords

buried pipeline, rockfall impact, finite element simulation, dynamic reliability.

1. Introduction

Due to its high efficiency and low transportation cost, pipeline has been widely used to transport natural gas and petroleum. For long-distance pipeline, it needs to pass through various types of terrains, and a variety of factors (such as landslide, collapse, and rockfall, etc.) can affect its performance and reliability [4]. Up to now, lots of rock impact events have occurred on pipeline, and they have seriously threatened the pipeline's safe operation [35]. To ensure the safe operation of buried pipeline, it is of great significance to analyze the pipeline's deformation mechanism and dynamic response, and further to predict the pipeline's reliability under rockfall impact [12, 26].

Affected by the ground motions, such as landslide or explosion, buried pipeline is vulnerable to rockfall impacts. Considering the dynamic interaction between the soil and pipeline, Manolis et al. [16] used the waveguide model in classical elastodynamics to study the dynamic response of continuous pipeline. To analyze the effect of spatial variability on the response of buried pipeline, Han et al. [6] conducted a series of three-dimensional shaking table tests to study the effect of non-uniform seismic excitation on pipeline's strain. By using the integral probability method, Xu et al. [28] deduced analytical formulas for the pipeline's deformation and axial stress caused by the friction of pipe and soil, and pipeline's stress and deformation along the mining process were analyzed. On the basis of linear viscoelasticity, Khusainov [11] established a pipe-soil interaction model, and the buried pipeline's dynamic response to a longitudinal wave propagating was analyzed. However, the above analytical models have not considered the axial and circumferential response of the buried pipeline under load impact.

Essentially, the deformation mechanism for the buried pipeline under rockfall impact is a nonlinear contact problem. Even the theoretical calculation formula can provide a simple solution, the obtained result has obvious limitations, especially on the accuracy and the range of application. In recent years, finite elements method (FEM) has received attention in this area. Ismail et al. [7] used FEM to evaluate the influence of pipeline's diameter, buried depth, wall thickness and other parameters on the resistance to upheaval buckling of buried submarine pipeline. Zhang et al. [33] analyzed the pipeline's deformation caused by radial impact, inclined impact, and eccentric impact of spherical rockfall and cubic rockfall. The results indicated that the smaller the curvature radius of the rockfall contact area is, the greater the damage to the pipeline will be. Shin et al. [21] applied

(*) Corresponding author.
(#) These authors contributed equally to this work.

E-mail addresses: C. Su (ORCID: 0000-0002-5523-1469): suchun@seu.edu.cn, Y. F. Wang : yifeiwang@seu.edu.cn, M.J. Xie : mingjiang@seu.edu.cn

FEM to study the interaction between pipe-soil-rock in the case of anchor impact. Meanwhile, the pipeline's strain caused by the change of anchor weights (drop heights), submarine pipeline buried depth and rock berm heights was obtained through experiments. Zhang et al. [32] established a pipe-soil finite elements model for buried pipeline, and the effects of the impact height, the pipe's wall thickness as well as the pipe's buried depth were studied. Aiming at the X80 steel large-diameter oil and gas pipeline crossing seismic faults, Yan et al. [29] employed a large deformation shell FEM to study the strain response, and the sensitivity of multiple impact factors on the pipeline was conducted. Jiang et al. [8] studied pipeline's response to the transverse impact load of falling objects, and the effects of various parameters on the pipeline were analyzed, including the seabed flexibility, buried depth and soil properties. Tian et al. [22] applied a nonlinear explicit dynamic FEM to assess the damage of the submarine pipeline under the impact of falling objects. Up to now, most studies focused mainly on the load impact on the pipeline's mechanical behavior, while the load impact on the pipeline's corrosion defects has rarely been studied.

For pipeline, the load impact usually results in corresponding deformation and further influences its reliability. In the last decades, numerical simulation methods have been widely applied to evaluate pipeline's reliability under the impact load. Zelmati et al [30] proposed a probabilistic method to evaluate the corroded pipeline's remaining life, and FEM was used to calculate the pipeline's failure pressure. Based on FEM, Abyani et al. [1] proposed a new method to evaluate the reliability of pipeline corrosion resistance. Then, the Latin hypercube sampling method was combined with simulated annealing to simulate the uncertainty of the random parameter. Aryai et al. [2] used the three-dimensional nonlinear FEM to model the residual strength of the pipeline in terms of time, and solved the reliability of the water pipe based on the time-dependent reliability analysis. Nahal et al. [17] studied the influence of corrosion and residual stress on the irregular area of the pipeline by establishing finite elements model of the corroded elbow area. The failure probability and reliability index of different corrosion areas were calculated by Monte Carlo simulation (MCS). In addition to using FEM, some studies used other reliability theories and mechanical models to study the influence of load on the pipeline's reliability. Zha et al. [31] studied the influence of traffic load on the reliability of buried polyethylene pipeline, where the center point method and MCS method were applied, and the reliability index and residual life of the buried pipeline were calculated. Li et al. [13] adopted Timoshenko beam and Winkler foundation model to analyze the performance of pipeline, and the pipeline's reliability was estimated with the method of subset simulation (SS). Guillal et al. [5] used the SS approach to study the reliability of medium-strength and high-strength pipeline under the plastic failure and fracture. Sahraoui et al. [20] investigated the effect of the repair for welded joint on the corroded pipeline's reliability considering the spatial variability of hardness and soil erosion.

Up to now, some works have been done regarding the buried pipeline under the impact load, including earthquake, explosion, traffic load, rockfall, etc. However, few studies have analyzed the residual life of buried steel pipes with corrosion defects, and the impact of rockfall is rarely considered. Moreover, the existing methods have not considered the coupling relationship among the dynamic response of buried corroded pipeline and the rockfall's parameters, such as rockfall mass, impact velocity and the impact position.

This study is to evaluate buried pipeline's reliability by considering the coupling relationship among the aforementioned factors. The major contributions are as follows: (1) The effect of rockfall parameters on the pipeline's deformation is analyzed, including rockfall mass, impact velocity, and impact position. Meanwhile, the coupling relationship between the von Mises equivalent stress and rockfall parameters is quantitatively analyzed; (2) Sensitivity analyses are conducted for the rockfall parameters, and dynamic reliability model is established to update the pipeline's reliability; (3) The pipeline's dynamic reliability during and after the rockfall impact are studied. This study can be used to evaluate the buried corroded pipeline's reliability considering the rockfall impact.

The remainder of the paper is organized as follows. Section 2 establishes the mechanical modeling of buried pipeline impacted by the external load. In Section 3, the dynamic reliability modeling of the buried pipeline under rockfall impact is introduced. The numerical model of the pipeline under the rockfall impact is established by FEM in Section 4, and the sensitivity analysis of various rockfall parameters is conducted. The accuracy and effectiveness of the proposed method is demonstrated through a case study in Section 5. Conclusions are given in Section 6.

2. Mechanism analysis of impact process

The impact process of the rockfall on the pipeline is quite complicated. It needs to be simplified in theoretical aspect, such as transforming it into a static problem for analysis. By taking the rockfall impact force as the static load, we can analyze the pipeline's stress. Up to now, two types of models can be used to describe the stress load of buried pipeline, i.e. multi-span continuous beam and elastic foundation beam [22]. In this study, we simplify the buried pipeline into an Euler-Bernoulli beam model to analyze the vibration response and the pipeline's characteristics under the impact load. To determine the pipeline's dynamic response under the rockfall impact, besides the initial boundary conditions, it also needs to quantify the impact force.

According to the theorem of kinetic energy, during the process of rockfall collision the energy loss (i.e ΔE) can be calculated as [10]:

$$\Delta E=\frac{1}{2}mv_0^2-\frac{1}{2}mv_1^2 \tag{1}$$

where m is the mass of rockfall; v_0 and v_1 are the initial and final velocities of the rockfall impact process respectively.

For the soil, its elastic deformation potential energy (i.e. W) can be expressed as:

$$W=\frac{1}{2}k\zeta^2 \tag{2}$$

where k is the stiffness of the soil spring; and ζ is the deformation value of the soil.

By now, three types of soil spring models are commonly applied, they are the pipe axial soil spring, horizontal soil spring, and vertical soil spring respectively. According to the standard of American Society of Civil Engineers (ASCE), the stiffness coefficients of the above three soil springs are as follows [29].

(1) Along the pipe axis, the friction f of the pipe per unit length is:

$$f=0.75\pi Dh\gamma_s\mu \tag{3}$$

where D is the diameter of the pipe; h is the distance from the central axis of the pipeline to the surface; γ_s is the unit weight of soil; and μ is soil friction coefficient of the pipe.

(2) In the horizontal lateral direction, the lateral earth pressure on the unit length of pipe (i.e. P) is given as:

$$P=\gamma_s hN_h D \tag{4}$$

where N_h is the horizontal bearing capacity coefficient of the sand.

(3) In the vertical direction, the soil reaction force on unit length of pipe (i.e. Q) is:

$$Q = \gamma_s h N_v D \tag{5}$$

where N_v is the vertical bearing capacity coefficient of the sand.

According to Eqs. (3) - (5), the values of the stiffness (i.e. k) for different types of soil springs can be obtained, and the elastic potential energy (i.e. W) can be calculated. Based on the law of conservation of energy, we have:

$$\Delta E = W \tag{6}$$

When the mass velocity (i.e. v) and the stiffness of the soil spring (i.e. k) are known, we can obtain the maximum deformation (i.e. $\zeta_{\max}$) with Eqs. (1)-(6). When the rockfall velocity is 0, the impact force on the soil will be the largest and the corresponding deformation is also the largest. The maximum impact force (i.e. F_{max}) can be expressed as:

$$F_{\max} = k\zeta_{\max} \tag{7}$$

Here, the Euler Bernoulli foundation beam is used to model the buried pipeline. Under the load impact of $Q(x, t)$, the differential equation for the pipeline's vibration (i.e. $y(x, t)$) can be obtained as [16]:

$$A\frac{\partial^4 y(x,t)}{\partial x^4} + m\frac{\partial^2 y(x,t)}{\partial t^2} + c\frac{\partial y(x,t)}{\partial t} + Ky(x,t) = Q(x,t) \tag{8}$$

where $y(x, t)$ is the pipeline's vibration; A is the bending stiffness of the pipeline; m is pipeline mass; c is foundation damping coefficient; and K is the foundation modulus.

The initial conditions and boundary conditions are defined in Eqs. (9) and (10), respectively.

$$y(x,t)\big|_{t=0} = \frac{\partial y(x,t)}{\partial t}\Big|_{t=0} = 0 \tag{9}$$

$$\lim_{x\to\infty} \frac{\partial^n y(x,t)}{\partial x^n} = 0 \left(n = 0,1,2,3\right) \tag{10}$$

During the process of impact, the pipeline is mainly affected by a series of short pulse loads. The unit pulse function is defined as:

$$\delta(x,x_0) = \begin{cases} 0, x \neq x_0 \\ \infty, x = x_0 \end{cases} \tag{11}$$

According to the Dirichlet condition, the function needs to satisfy the following items [3]: (1) There are only finite discontinuities of the first kind (both left and right limits exist) in a continuous field; (2) If there are only finite extreme points, the function can be expanded into Fourier series. When δ satisfies the conditions, it can be expanded as:

$$\delta(x,x_0) = \frac{2}{T}\sum_{n=1}^{\infty} \sin\left(\frac{n\pi}{T}x\right)\cdot\sin\left(\frac{n\pi}{T}x_0\right) \tag{12}$$

The unit concentrated impulse is:

$$Q_0(x,t) = \delta(x,x_0)\delta(t,t_0) = \frac{2}{T}\sum_{n=1}^{\infty} \sin\left(\frac{n\pi}{T}x\right)\cdot\sin\left(\frac{n\pi}{T}x_0\right)\cdot\delta(t,t_0) \tag{13}$$

$$Q(x,t) = F_{\max}\cdot Q_0(x,t) \tag{14}$$

The solution for Eq. (8) can be expressed as the follows:

$$y(x,t) = \sum_{n=1}^{\infty} y_n(t)\cdot\sin\left(\frac{n\pi}{T}x\right) \tag{15}$$

Bring Eq. (15) into Eq. (8), we have:

$$\sum_{n=1}^{\infty} A\left|\frac{n\pi}{T}\right|^4 y_n(t)\sin\left(\frac{n\pi}{T}x\right) + \sum_{n=1}^{\infty} m\ddot{y}_n(t)\sin\left(\frac{n\pi}{T}x\right) + \sum_{n=1}^{\infty} C\dot{y}_n(t)\sin\left(\frac{n\pi}{T}x\right) + \sum_{n=1}^{\infty} k y_n(t)\sin\left(\frac{n\pi}{T}x\right) = \frac{2}{T}F_{\max}\sum_{n=1}^{\infty}\sin\left(\frac{n\pi}{T}x\right)\sin\left(\frac{n\pi}{T}x_0\right)\delta(t,t_0) \tag{16}$$

Moreover, it can be simplified as:

$$\ddot{y}_n(t) + c\dot{y}_n(t) + p^2 y_n(t) = \gamma(t) \tag{17}$$

where $c = \frac{C}{m}$; $p^2 = \frac{1}{m}\left(\left|\frac{A}{T}\right|^4 + k\right)$; and $\gamma(t) = \frac{2F_{\max}}{mT}\sin\left(\frac{n\pi}{T}x_0\right)\delta(t,t_0)$.

The general solution for homogeneous equation y_n^* is:

$$y_n^* = e^{-\frac{c}{2}t}\left(C_1\cos\left(\sqrt{p^2 - \frac{c^2}{4}}\right)t + C_2\sin\left(\sqrt{p^2 - \frac{c^2}{4}}\right)t\right) \tag{18}$$

where C_1 and C_2 are the constants.

The particular solution $\bar{y}_n$ of the inhomogeneous equation can be obtained by using undetermined coefficient method:

$$\bar{y}_n = \frac{2}{mT}\sin\left(\frac{n\pi}{T}x_0\right)e^{-\frac{c}{2}(t-t_0)}\sin\left(\sqrt{p^2 - \frac{c^2}{4}}(t-t_0)\right) \tag{19}$$

The solution of vibration control differential equation for the buried pipeline under unit external force is as follows:

$$y(x,t) = \sum_{n=1}^{\infty} F_{\max}e^{-\frac{c}{2}t}\left|C_1\cos\left(\sqrt{p^2 - \frac{c^2}{4}}\right)t + C_2\sin\left(\sqrt{p^2 - \frac{c^2}{4}}\right)t + \frac{2}{mT}\sin\left(\frac{n\pi}{T}x_0\right)e^{\frac{c}{2}(t-t_0)}\sin\left(\sqrt{p^2 - \frac{c^2}{4}}\right)(t-t_0)\right|\sin\frac{n\pi}{T}x \tag{20}$$

Therefore, to analyze the dynamic response of the buried pipeline under external load, we can establish the foundation beam model under impact load, on the basis of unit pulse function and Fourier series. By analytically calculating of the model, we can obtain the pipeline's displacement and velocity response. So far, the mechanical parameters are obtained, including the pipeline's bending moment and shear force.

3. Structural reliability theory

The pipeline's stress and strength are essentially random variables, and we can define them with the probability distributions. At the initial stage of usage, the strength is usually greater than the stress, thus the pipeline has sufficient safety margin. With the increase of the pipeline's service life, and under the influence of corrosion defect and other factors, the pipeline's strength will decrease gradually. When the strength is lower than the stress, failure will occur. Therefore, we

can define the pipeline's limit state function (LSF), i.e. G as follows [36]:

$$G = H - S \tag{21}$$

where H is the generalized strength, and it indicates the pipeline's bearing capacity; and S denotes the generalized stress.

According to the value of G, the pipeline has three types of states: (1) $G = 0$, it indicates that the pipeline is in a limit state; (2) $G > 0$, it indicates that the pipeline is in reliable state; and (3) $G < 0$, it indicates that the pipeline is in failure state [24]. Therefore, the pipeline's failure probability (i.e. P_f) can be written as:

$$P_f = P\left(G = H - S < 0\right) \tag{22}$$

3.1. Limit state functions

3.1.1. Model of burst failure

For buried pipeline, when the operating pressure exceeds the allowable pressure, the pipeline will burst. Here, based on Eq. (21), we can rewrite the pipeline's LSF as follows:

$$G_1(t) = P_b - P_0 \tag{23}$$

where P_b is the pipeline's burst pressure; and P_0 is the pipeline's operation pressure.

In this study, the DNV RP-F101 model is adopted [27], and P_b is estimated with:

$$P_b = \frac{2\omega U}{D-\omega}\left[\frac{1-\frac{d}{\omega}}{1-\frac{d}{\omega M}}\right] \tag{24}$$

where U is the ultimate tensile strength of the pipeline; ω is the pipe wall thickness; d is corrosion depth; D is the outer diameter of the pipe; l is the length of the corrosion defect; and M is the expansion coefficient of the pipeline.

$$M = \sqrt{1 + 0.31\frac{l^2}{D\omega}} \tag{25}$$

3.1.2. Von Mises stress failure model

For the buried corroded pipeline, it needs to bear various types of loads, including the internal pressure, soil covering, and potential rockfall impact, etc. The loads may cause deformation of the pipeline, thus it will affect the pipeline's safe operation. Eq. (21) can be rewritten in stress failure mode, as follows [25]:

$$G_2 = \sigma_y - \sigma_e \tag{26}$$

where σ_y is the yield strength of pipeline material; and σ_e is the equivalent stress caused by loads.

According to von Mises stress theory, the equivalent stress (i.e. σ_e) can be expressed as [14, 19]:

$$\sigma_e = \sqrt{\sigma_c^2 + \sigma_l^2 - \sigma_c\sigma_l} \tag{27}$$

where σ_c is the circumferential stress of buried corroded pipeline; and σ_l is the axial stress.

3.2. Calculation of pipeline's failure probability

In this study, two types of failure modes are considered for the buried pipeline, i.e. burst pressure and von Mises stress failure. Therefore, the pipeline's failure probability can be expressed as [18]:

$$P_f(t) = P\left[G_1(t) \le 0 \cup G_2(t) \le 0\right] \tag{28}$$

where G_1, G_2 are the LSFs of the above failure modes respectively.

3.3. Simulation method

The basic procedures for calculating the pipeline's failure probability with MCS are as follows [15]:

(1) Set the total number of simulations (i.e. N) to analyze the failure probability of the corroded pipeline;
(2) Based on the pipeline's historical statistical data, determine the mean and standard deviation of each variable;
(3) By using the statistical characteristics of the random variables in Step (2), generate the samples;
(4) Substitute the generated samples into LSFs, and count the number of LSFs that is less than 0 (i.e. N_f);
(5) Calculate the pipeline's failure probability (i.e. p_f), by using Eq. (29):

$$p_f = \frac{N_f}{N} \tag{29}$$

where N_f is the number of simulations in violation of LSF (i.e., the LSF is less than zero).

3.4. Reliability analysis for buried corroded pipeline under rockfall impact

On the basis of the reliability theory and Eqs. (21)-(28), we can obtain the probability of failure of the event (i.e. p_i) as follows:

$$P_i(t) = P\left(G_i\left(H_i, S_i, t\right) < 0\right) = P\left(H_i(t) < S_i(t)\right) \tag{30}$$

where $P_i(t)$ denotes the probability of an event; $S_i(t)$ denotes the structural response (i.e., load effects); $H_i(t)$ denotes the structural resistance; and G_i is the LSF, it is defined as $G_i = H_i(t) - S_i(t)$.

Considering the process of the rockfall impact on the buried pipeline, the first time that the rockfall impact usually has the most serious harm to the pipeline. In dynamic reliability theory, it also satisfies the first transcendental failure mechanism. It can be regarded as "first passage probability", and the corresponding expression is as follows [9]:

$$p_f(t) = 1 - \left[1 - p_f(0)\right]e^{-\int_0^t \nu dt} \tag{31}$$

where $p_f(0)$ is the failure probability at time $t=0$; and ν is the mean rate for the response process $S(t)$ to upcross the threshold $H(t)$.

The upcrossing rate (i.e. ν) can be determined by Rice formula [23]:

$$\nu = \nu_H^+ = \int_H^\infty \left(\dot{S} - \dot{H}\right) f_{S\dot{S}}\left(H, \dot{S}\right) d\dot{S} \tag{32}$$

where v_H^+ is the upcrossing rate of the response process S(t) relative to the resistance threshold process threshold H; $\dot{H}$ is the slope of H relative to time t; $\dot{S}(t)$ is the time derivative process of $S(t)$; and $f_{S\dot{S}}(\cdot)$ is the joint probability density function of S and $\dot{S}$:

$$v = v_{H=d}^{+} = \frac{\sigma_{\dot{S}|S}}{\sigma_S}\phi\left(\frac{H-\mu_S}{\sigma_S}\right)\left\{\phi\left(\frac{\dot{H}-\mu_{\dot{S}|S}}{\sigma_{\dot{S}|S}}\right)-\frac{\dot{H}-\mu_{\dot{S}|S}}{\sigma_{\dot{S}|S}}\Phi\left(-\frac{\dot{H}-\mu_{\dot{S}|S}}{\sigma_{\dot{S}|S}}\right)\right\} \tag{33}$$

where $v_{H=d}^+$ is the upcrossing rate relative to deterministic threshold H; $\phi(\cdot)$ and $\Phi(\cdot)$ are the standard normal density and distribution functions respectively; μ and σ are the mean and standard deviation of S and $\dot{S}$.

When the response process obeys Gaussian process, its mean function (i.e. $\mu_s(t)$) and auto-covariance (i.e. $C_{ss}(t_i,t_j)$) can be determined by the Eqs. (34) - (39) [23]:

$$\mu_{\dot{S}|S} = E\left[\dot{S}|S=H\right] = \mu_{\dot{S}} + \rho_S\frac{\sigma_{\dot{S}}}{\sigma_S}\left[H-\mu_S\right] \tag{34}$$

$$\sigma_{\dot{S}|S} = \sqrt{\sigma_{\dot{S}}^2\left(1-\rho_S^2\right)} \tag{35}$$

where:

$$\mu_{\dot{S}} = \frac{d\mu_s(t)}{dt} \tag{36}$$

$$\sigma_{\dot{S}} = \sqrt{\frac{\partial^2 C_{SS}(t_i,t_j)}{\partial t_i \partial t_j}|i=j} \tag{37}$$

$$\rho_S = \frac{C_{S\dot{S}}(t_i,t_j)}{\sqrt{C_{SS}(t_i,t_j)C_{\dot{S}\dot{S}}(t_i,t_j)}} \tag{38}$$

and the cross-covariance function is:

$$C_{S\dot{S}}(t_i,t_j) = \frac{\partial C_{SS}(t_i,t_j)}{\partial t_j} \tag{39}$$

On this basis, we can determine all the variables in Eq. (33).

For a clear illustration, the analysis process can be divided into four parts, they are: (1) mechanism analysis of impact process; (2) pipeline's reliability modeling; (3) simulation with FEM: and (4) case study, respectively. The framework is shown as in Fig. 1.

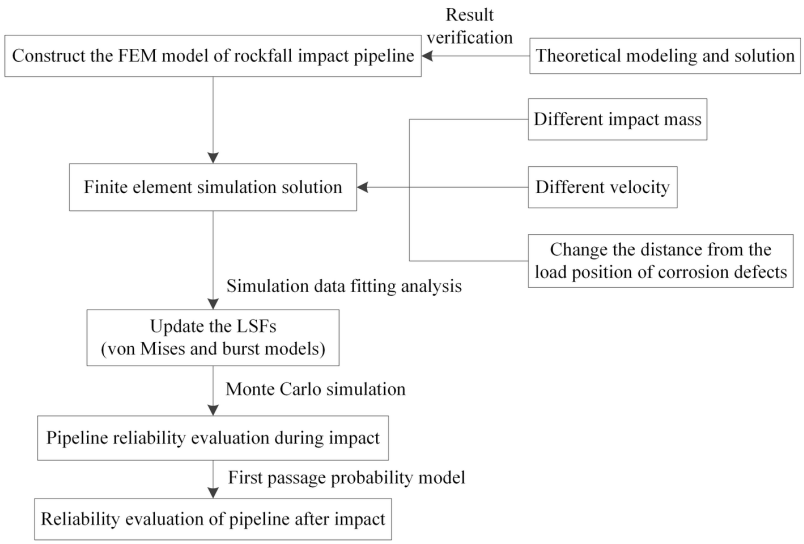

Fig. 1. Flow chart of the proposed approach

4. Finite element model

In this study, by using the finite element analysis software of ABAQUS, a three-dimensional FEM of the pipeline-soil-rockfall is established, and it is used to analyze the rockfall impact on buried corroded pipeline. In this model, the rockfall is assumed to impact the soil vertically to the tangent plane of the defect length.

4.1. Parameters of the material

In the FEM model, the length of the pipeline is set to be 10m, and the length of the rockfall is set as 320 mm. Besides, the size of the stratum is 10 m×4 m×4 m, and the thickness of backfill soil is 1m. The ideal elastic-plastic Drucker-Prager constitutive model [32] is adopted to describe the mechanical behavior of stratum and rock materials. The other parameters for the pipeline, soil, and rockfall are shown as in Table 1 and Table 2 respectively [34]. Moreover, the dilation angles of the soil and rock are set to be zero.

Table 1. Parameters of the pipeline

Diameter (mm)	Wall thickness (mm)	Density (kg/m^3)	Poisson's ratio	Young's modulus (MPa)	Yield strength (MPa)
813.00	8.00	7800.00	0.30	2.06×10^5	448.50

Table 2. Parameters of the soil and rockfall

Material type	Density (kg/m^3)	Poisson's ratio	Elastic modulus (MPa)	Internal friction angle (°)	Cohesion (MPa)
Soil	1840.00	0.30	20.00	15.00	0.015
Rockfall	2800.00	0.30	2.85×10^5	42.00	6.72

4.2. Geometric modeling

The geometric models are established for the rockfall, soil, and pipeline respectively, as shown in Fig. 2. The falling rock is represented by a cube, and the soil is modeled with a cuboid hollowed out in the middle, as shown in Fig. 2(a). The eight-node hexahedron linear reduced integral solid element (i.e. C3D8R) is adopted for the pipeline and soil respectively. Moreover, to obtain accurate simulation results, it needs to refine the mesh locally. On this basis, the dense grids are arranged at the defected parts, and at the intact parts coarse meshes are used, as shown in Figs 2(b) respectively.

4.3. Contact and boundary setting

In the finite elements model, two types of contact pairs are defined, they are the contact pair between the pipeline and soil, and the contact pair between the rockfall and soil, respectively. Moreover, it is assumed that the buried soil belongs to large granular sand, and the soil's friction coefficient is 2.5. Both the contact pairs are surface to surface

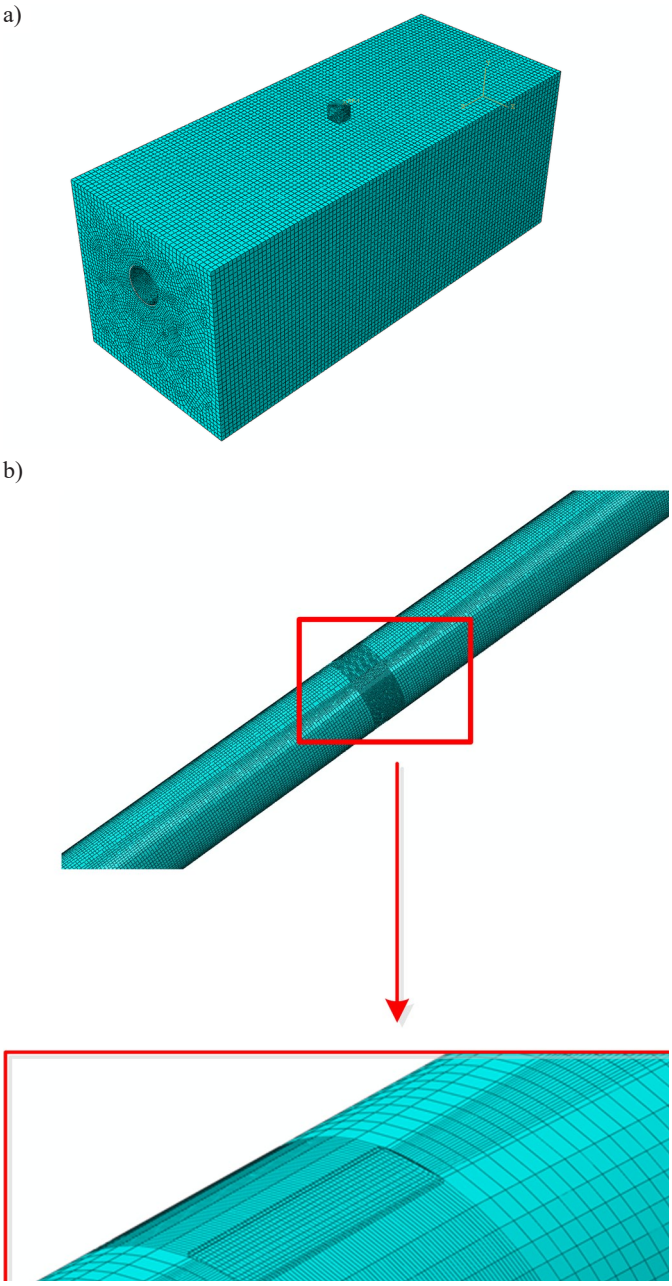

Fig. 2. Finite element model for the pipeline: a) finite element model of pipe-soil-rockfall, b) mesh division of the pipeline and enlargement of the defect's mesh

(explicit) contacts, and the penalty function algorithm is adopted. Moreover, in order to simplify the simulation process, this paper selects a single pipe as the research object, where the influence of pipe connection on the simulation results is ignored [34]. Within the impact model, three types of factors are considered in the boundary conditions, they are: (1) limit the rigid displacement of the pipeline along the vertical direction of the soil, and the soil's bottom boundary is set as a fixed one; (2) set the soil and pipeline's section symmetrical boundary conditions; (3) the rockfall is restrained, and it can move only vertically along the soil.

5. Results and discussion

5.1. Parameter determination

In this section, to demonstrate the effectiveness of the proposed method, numerical cases are conducted to analyze the dynamic response and reliability variation for the pipeline with corrosion defects and under the rockfall impact. The diameter of the APIX80 pipeline is 813 mm, the wall's thickness is 8 mm, and the yield strength is 448.5 Mpa. To facilitate the research, the corrosion defects are appropriately simplified. It is assumed that the shape of the corrosion defect is cuboid, and the size of the corrosion defect is 400 mm×200 mm×4 mm. The falling rock is cubic, and its side length is 320 mm. The buried depth of the pipeline is 1m. In total, 395 times of simulations are done, where the rockfall impact velocity increases from 10 m/s to 30 m/s, with an increment of 5 m/s; the rockfall mass increases from 68.9 kg to 160.7 kg, with an increment of 22.9 kg; the axial distance from the impact position to the corrosion center moves from 0mm to 2500 mm with an increment of 625 mm each time; the corrosion length is from 200 mm to 600 mm with an increment of 100 mm; the corrosion width is from 100 mm to 300 mm with an increment of 50 mm; and the corrosion depth is from 2 mm to 6 mm with an increment of 1 mm.

5.2. Validation of finite element model

By using the parameters introduced in Section 5.1 and comparing the result with the theoretical model introduced in Section 2, the effectiveness of the proposed FEM simulation model is demonstrated. The displacement response curves of the theoretical solution and FEM simulation are shown in Fig. 3. It is found that the results obtained with the two types of methods are quite close, and the maximum error is around 9%. Further, it is more convenient to apply FEM to analyze the rockfall impact on buried corroded pipeline's dynamic reliability. Subsequently, the reliability of the buried pipeline will be evaluated and updated through a large number of FEM simulation data.

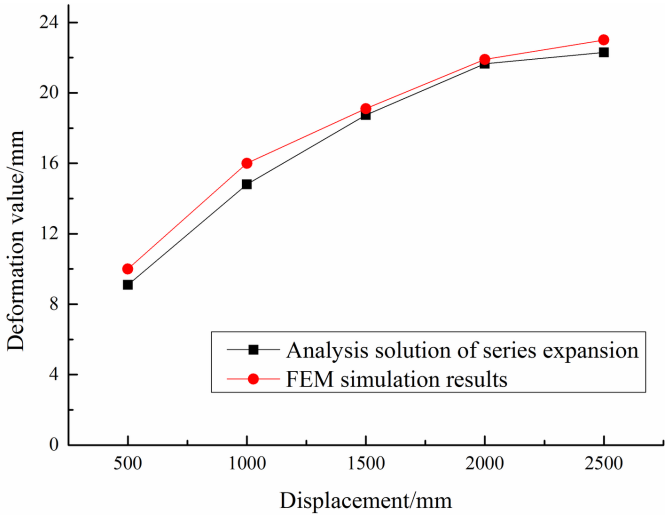

Fig. 3. Displacement response results of FEM simulation and theoretical solution

5.3. Parameters analysis of rockfall impact

Here, the rockfall mass is assumed to be 160.7 kg, the impact velocity is 20 m/s, and the axial distance to the center of the corrosion defect is 2500 mm. With respect to different impact times, the impact analysis results are shown in Fig. 4. Figs. 4(a)-(b) show the falling contact process of rockfall impact. The radial displacement results show that the rockfall only contacts with the soil in 0s and reaches the deepest point in 0.01s. Meanwhile, the rockfall has moved 152.7 mm downward. Figs. 4(c)-(f) show the rebound process after the rockfall hitting against the deepest point. It is found that the rockfall rebounds upward at 0.02s and moves upward by 47.8 mm. Moreover, the trend is more obvious at 0.05s, where the rockfall moves upward by 166.2 mm.

A large number of simulations are carried out to analyze the influence of rockfall masses, velocities and axial distances on the corrosion defect. Table 3 lists some of the results of the simulation.

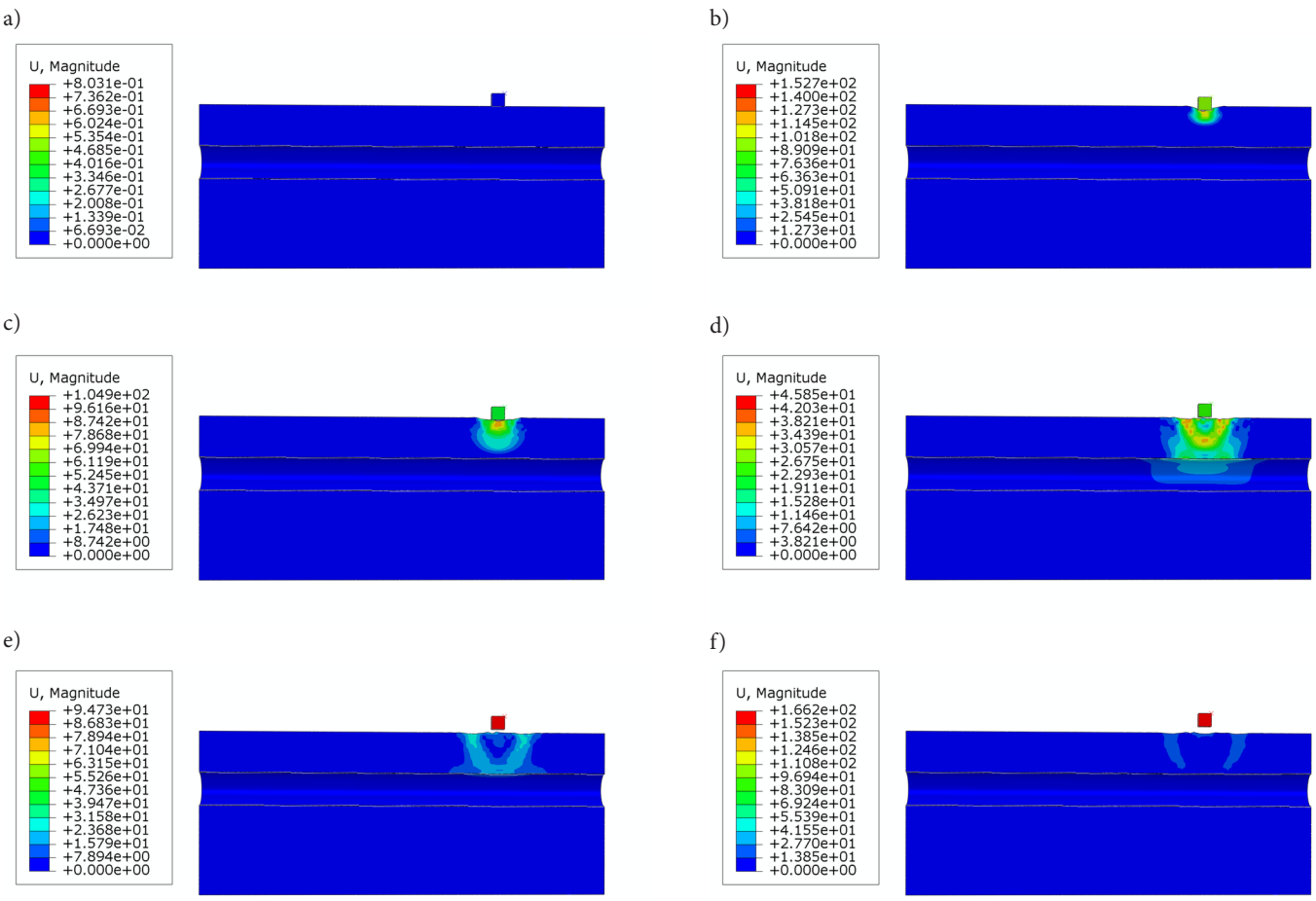

Fig. 4. Variation of rockfall radial displacement during impact: a) the impact time is 0s, b) the impact time is 0.01s, c) the impact time is 0.02s, d) the impact time is 0.03s, e) the impact time is 0.04s, f) the impact time is 0.05s

Table 3. Simulation results under different parameters of rockfall

Rockfall mass (kg)	Rockfall velocity (m/s)	Axial distance from corrosion defect (mm)	Von Mises (MPa)
68.90	10.00	0.00	335.60
68.90	20.00	0.00	354.20
68.90	30.00	0.00	384.70
68.90	10.00	625.00	236.10
68.90	20.00	625.00	289.20
68.90	30.00	625.00	305.30
68.90	10.00	1250.00	227.70
68.90	20.00	1250.00	259.70
68.90	30.00	1250.00	284.60
68.90	10.00	1875.00	233.60
68.90	20.00	1875.00	264.30
68.90	30.00	1875.00	321.50
137.80	10.00	0.00	346.40
137.80	20.00	0.00	549.00
137.80	30.00	0.00	677.50
137.80	10.00	625.00	335.50
137.80	20.00	625.00	538.00
137.80	30.00	625.00	643.00
137.80	10.00	1250.00	323.20
137.80	20.00	1250.00	493.50
137.80	30.00	1250.00	616.20
137.80	10.00	1875.00	313.30
137.80	20.00	1875.00	514.20
137.80	30.00	1875.00	594.80

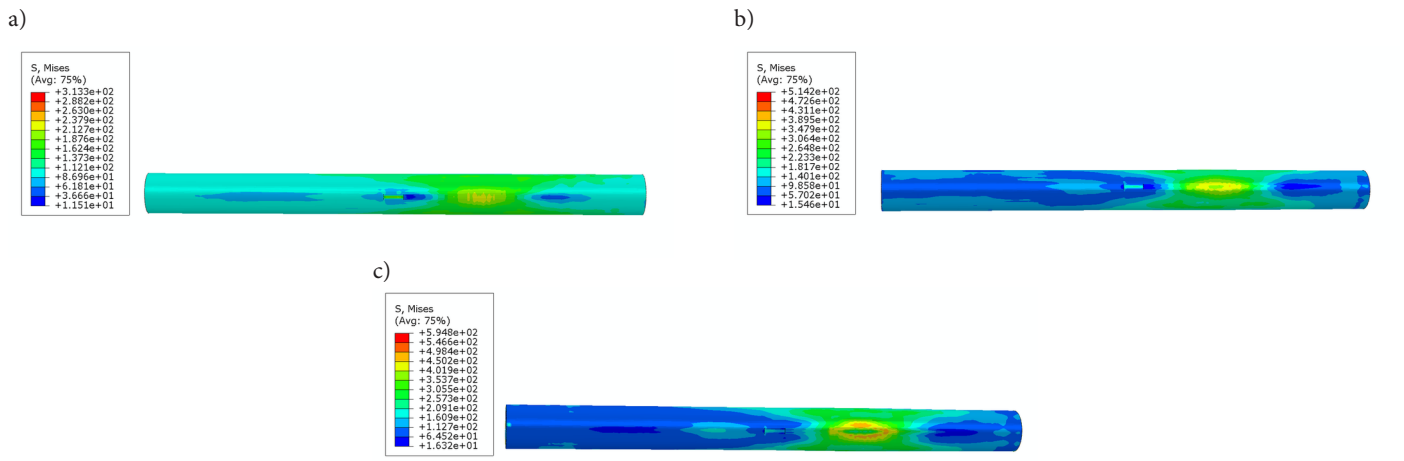

Fig. 5. Nephogram of pipeline's stress under different impact velocities: a) 10m/s, b) 20m/s, c) 30m/s

5.3.1. The effect of impact velocity

Fig. 5 shows the von Mises equivalent stress nephogram corresponding to the buried pipeline under the impact velocity from 10m/s to 30 m/s. The stress nephogram of changing rockfall mass and impact position is similar to that in Fig. 5. The results show that the pipeline's von Mises equivalent stress will increase with the increase of impact velocity. The reason is that the increase of impact velocity will increase the rockfall's energy impacting on the soil, which will increase the deformation of the buried pipeline. Meanwhile, since the strength of the corrosion defect is low, and the increase of the load will lead to the transfer of the maximum stress position.

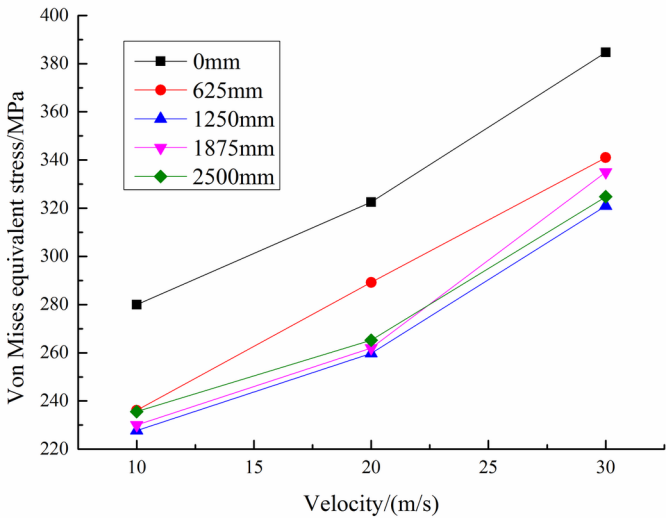

Fig. 6. The effect of impact velocity variation on von Mises equivalent stress

Fig. 6 indicates the relationship between the von Mises equivalent stress and the impact velocity under different axial distances. It is found that for buried pipeline, the von Mises equivalent stress increases with the increase of impact velocity, when the impact position is from 0 mm to 2500 mm. However, the relationship between the impact velocity and von Mises equivalent stress is not a simple linear growth relationship. The impact force increases with the increase of rockfall velocity, and the pipeline's peak stress will also increase. Meanwhile, as the impact position of rockfall will gradually move away from the corrosion defects, the von Mises equivalent stress will first decrease when the axial distance is within 0mm-1250 mm, and then increase when the axial distance is within 1250-2500 mm.

5.3.2. The effect of rockfall mass

Moreover, according to Eq. (1), the impact energy will increase with the increase of the rockfall's mass, and it will aggravate the pipeline's deformation and stress concentration. Fig. 7 shows the curves of the von Mises equivalent stress of the buried pipeline vs. the rockfall's mass with different velocities. Obviously, under the same impact velocity, the pipeline's von Mises equivalent stress will monotonously increase with rockfall mass. It is found that the larger the impact velocity, the larger the von Mises equivalent stress will be. When the rockfall mass exceeds a critical value, the peak of the pipeline's von Mises equivalent stress will exceed the yield strength, and finally result in the pipeline's failure.

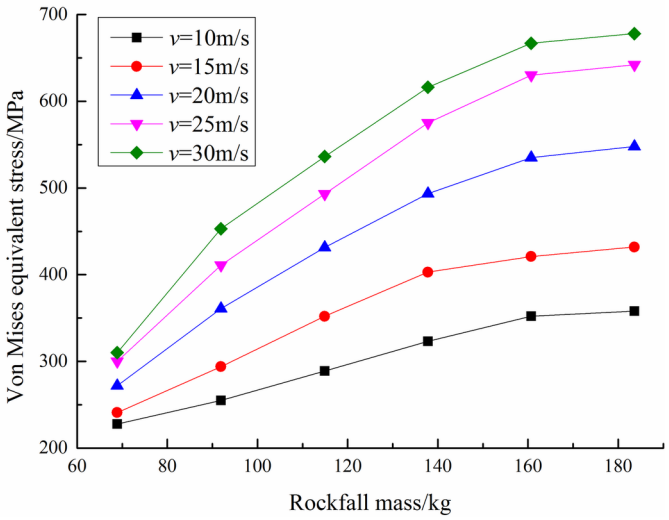

Fig. 7. Von Mises equivalent stress curve (impact position of 1250mm)

5.3.3. The effect of impact positions

Fig. 8 shows the curves of the von Mises equivalent stress under different impact positions and velocities. It is found that at the same impact position, the von Mises will increase with the increase of rockfall impact velocity. Meanwhile, as the position of the rockfall impact moves gradually away from the pipeline's defect, the von Mises equivalent stress will first decrease and then increase. Fig. 9 describes the relationship between the impact positions and the von Mises equivalent stress. Actually, it can help to explain the above results.

According to Fig. 9, when the rockfall mass is 68.9 kg and the impact velocity is 10 m/s, as the impact position of the rockfall moves gradually away from the defect center, the pipeline's corresponding position of von Mises equivalent stress changes greatly. Some conclusions can be gained as follows:

(1) When the impact position is at the defect center (i.e. 0 mm), the maximum stress will occur at the defect's edge. As the impact position increases from 0mm to 1250 mm, the maximum stress will gradu-

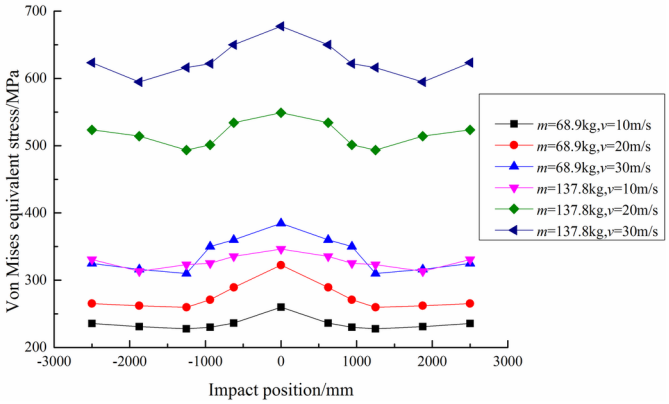

Fig. 8. The effect of impact position on von Mises equivalent stress

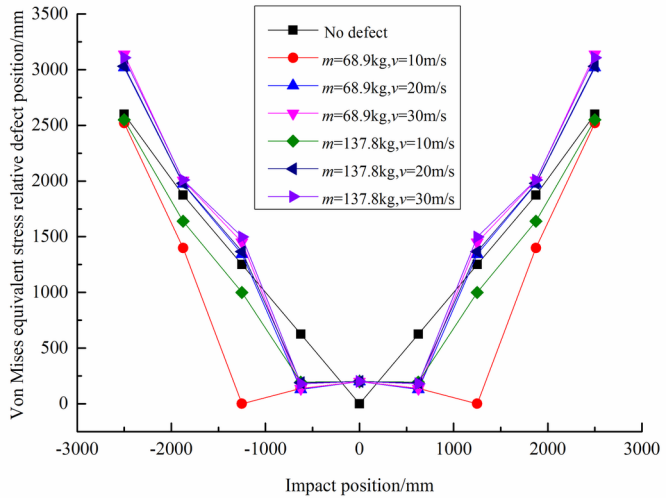

Fig. 9. The relationship between impact position and von Mises equivalent stress relative defect position

ally move to the defect center. With the further increase of the impact position, the position of the maximum stress will suddenly move to the impact position. In this study, the impact position that caused the sudden change of maximum stress position is defined as the critical impact position. When the rockfall mass is 68.9 kg and the impact velocity is 10m/s, the critical impact position is around 1250 mm. The reason is that the effect of the corrosion defects on the pipeline is weakened gradually, and the effect of the impact on the pipeline stress is larger than the defect.

(2) When the rockfall's mass remains unchanged and its velocity increases from 10 m/s to 30 m/s, the maximum stress is still at the edge of the defect, with the rockfall impact happening at the defect center. With the increase of the impact position, the maximum stress will also move to the impact's position. As the velocity of the impact becomes larger, the critical impact position becomes smaller. When the rockfall's mass is 137.8 kg, the curves for different velocities are similar while with smaller critical impact positions.

(3) When the impact energy is less than a certain threshold, and within the critical impact position, the maximum stress gradually moves from the defect edge to the defect center. When the impact position is larger than or equal to the critical impact position, the maximum stress position will move to the impact area.

According to Figs. 6-9, it is found that the impact mass, velocity, and the position of the rockfall impact will affect the results of the von Mises stress. To further evaluate the reliability of the buried pipeline under the rockfall impact, the relationship among these factors and the pipeline's von Mises equivalent stress needs to be investigated.

5.3.4. The effect of corrosion defect

The existence of pipeline corrosion defects will lead to the decrease of its strength. Therefore, in this section we study the influence of corrosion defect size on the von Mises equivalent stress of the pipeline. When the impact mass of rockfall is 91.8 kg and the impact position is 0mm, the analysis results are shown as in Fig. 10. Figs. 10 (a) and (b) show the stress diagrams corresponding to the change of defect length and width respectively. It can be found that the stress increases with the increase of defect length, while the increasing speed decreases gradually. The overall variation range of von Mises equivalent stress is very small, basically within 25 MPa. Meanwhile, when the impact velocity increases, the stress will increase accordingly. The change of corrosion defect width has the same trend. Fig. 10 (c) shows the effect of the change of defect depth on the stress. It can be seen that

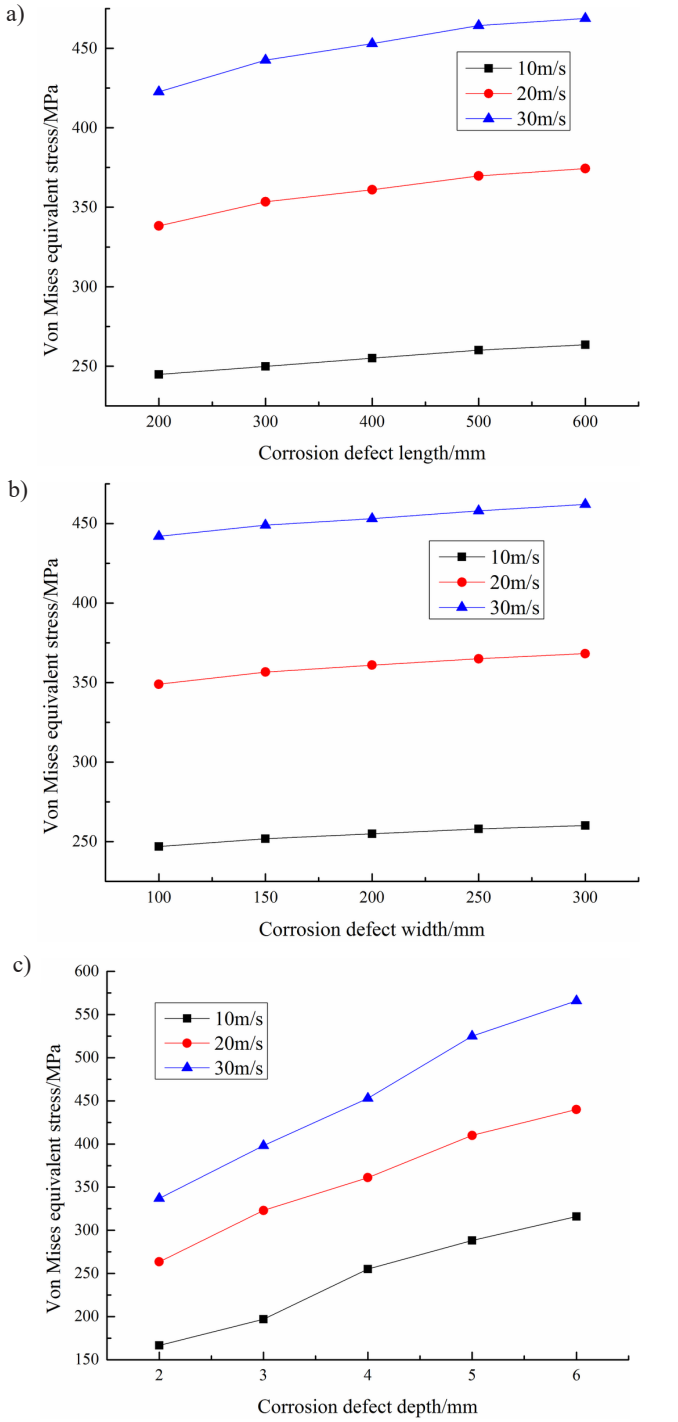

Fig. 10. The stress diagram of different corrosion defect geometry: a) different corrosion lengths, b) different corrosion widths, c) different corrosion depths

the stress increases with the increase of defect depth, which is almost linear. When the impact velocity is 30m/s, the overall variation range of von Mises equivalent stress amplitude reaches 229 MPa. Therefore, the equivalent stress of the pipeline is greatly affected by the defect depth.

5.4. Fitting of rockfall parameters

The coupling relationship among the mass, velocity, impact position and pipeline's maximum von Mises equivalent stress are shown in Fig. 11. From Fig. 11 (a), with the increase of the impact velocity and impact time, the von Mises equivalent stress continues to increase. The relationship among the rockfall mass, impact time and the von Mises equivalent stress are shown in Fig. 11 (b), and it has a similar trend as Fig. 11(a). Meanwhile, the effect of the rockfall impact's position on the von Mises equivalent stress is shown in Fig. 11(c). Obviously, compared with the rockfall mass and impact velocity, the effect of the rockfall impact's position on the von Mises equivalent stress is relatively small. Here, the polynomial function is used to fit the relationship among the rockfall mass, velocity, impact position, and the maximum equivalent stress of the pipeline. Moreover, by using the parameters fitting technique, the results can be quantified to update the corroded pipeline's reliability under the rockfall impact.

To better describe the change process of von Mises during impact, we draw the trend diagrams of stress and rockfall parameters under different parameters in Fig. 11. Among them, the change slope of von Mises can be obtained.

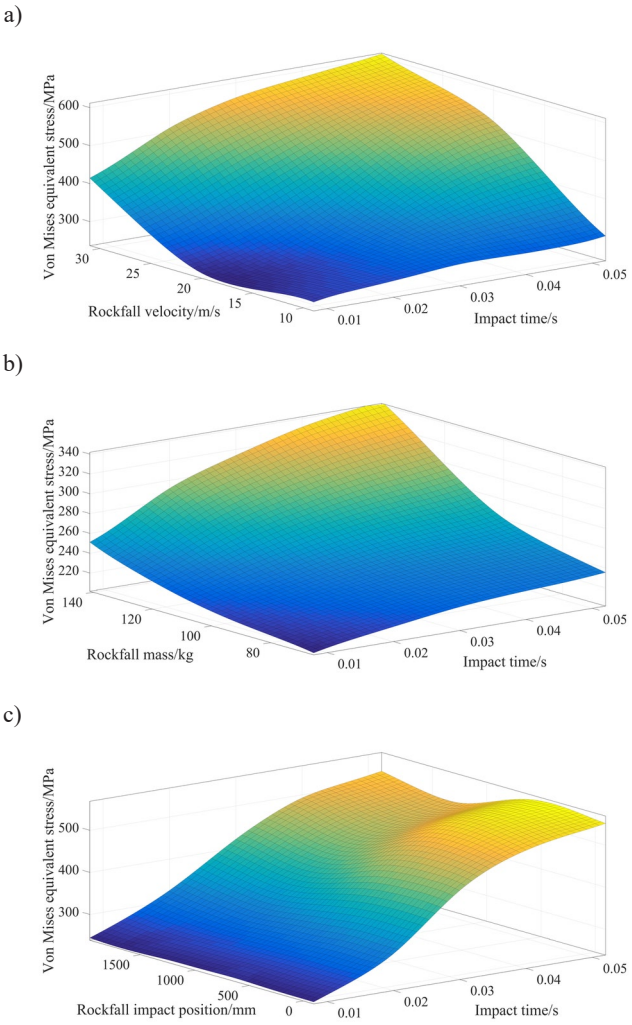

Fig. 11. Variation of the pipeline's von Mises equivalent stress under different parameters: a) Von Mises equivalent stress vs. impact velocity and impact time, b) Von Mises equivalent stress vs. rockfall mass and impact time, c) Von Mises equivalent stress vs. impact position and impact time

Here, R-squared (R^2) is used to evaluate the imitative effect of the fitting function, and it is shown as in Eq. (40) [37]:

$$R^2=\frac{\sum\left(\hat{y}_i-\bar{y}\right)^2}{\sum\left(y_i-\bar{y}\right)^2} \tag{40}$$

where y_i is the ith observation; $\bar{y}$ is the mean value of observed value; and $\hat{y}_i$ is the ith observation of linear regression.

After the impact time is 0.05s, the relationship between von Mises stress and rockfall mass, impact velocity and impact position is shown in the Fig.12.

Fig. 12 shows the relationship between rockfall parameters and stress after impact. Among it, Fig. 12 (a) shows the von Mises stress relationship corresponding to the change of rockfall mass and velocity when the impact position is 625 mm; Fig. 12(b) shows the stress contour map under different masses and velocities. When the velocity increases from 10 m/s to 30 m/s and the mass increases from 72 kg to 160 kg, the peak stress gradually increases from 100 MPa to 500 MPa. And the rockfall velocity has a greater impact on the stress. Fig. 12(c) indicates the relationship among the stress and the rockfall mass and the impact position when the impact velocity is 10m/s. The corresponding stress contour map is shown in Fig.12(d). As observed from Fig.12(c) and Fig.12(d), when the rockfall mass increases from 72 kg to 160 kg and the impact position increases from 0mm to 1800 mm, the peak stress changes from 100 MPa to 300 MPa. As the impact position varies from 600 mm to 1800 mm, the stress will decrease first and then increase. In this process, the stress amplitude changes little. The stress relation diagram corresponding to different rockfall velocities and impact positions when the rockfall mass is 68 kg are shown in Figs.12(e)-(f). When the rockfall velocity increases from 10m/s to 30 m/s and the impact position increases from 0mm to 2500 mm, the peak stress changes from 240 MPa to 380 MPa. The change of peak stress has a similar trend with that in Fig.12(c)-(d).

Through the analyses in Fig. 12, we find that both the rockfall mass and impact velocity have a positive correlation with von Mises stress, while the relationship between impact position and stress is relatively complicated. In order to better describe the relationship between these parameters and von Mises stress, artificial neural network (ANN) model is used in this paper. The rockfall mass, impact velocity and impact position are taken as input variables and stress as an output variable. The relationship among them is shown in Eq. (41). The finite element simulation data for selected factors are used to train the ANN model and the simulation data points are randomly divided into three sets: (1) 70% for training; (2) 15% for testing; and (3) 15% for validation. Through running multiple tests with different ANN model parameters, we find that when the number of input layers is 3, the number of hidden layers is 10 and the number of output layers is 1, the prediction accuracy of ANN model is the best. The predicted results are shown in Fig.13. It can be seen from the Fig.13 that the prediction accuracy of the ANN model is relatively high (R^2 is 0.9765). Subsequently, the von Mises equivalent stress results of the pipeline under different parameters can be predicted based on this model:

$$S=f\left(m,v,d\right) \tag{41}$$

5.5. Reliability analysis of buried corroded pipeline

As mentioned previously, when the rockfall contacts the soil for the first time, the impact energy is the largest, and the impact force on the underground pipeline is the largest. When the rockfall impacts the

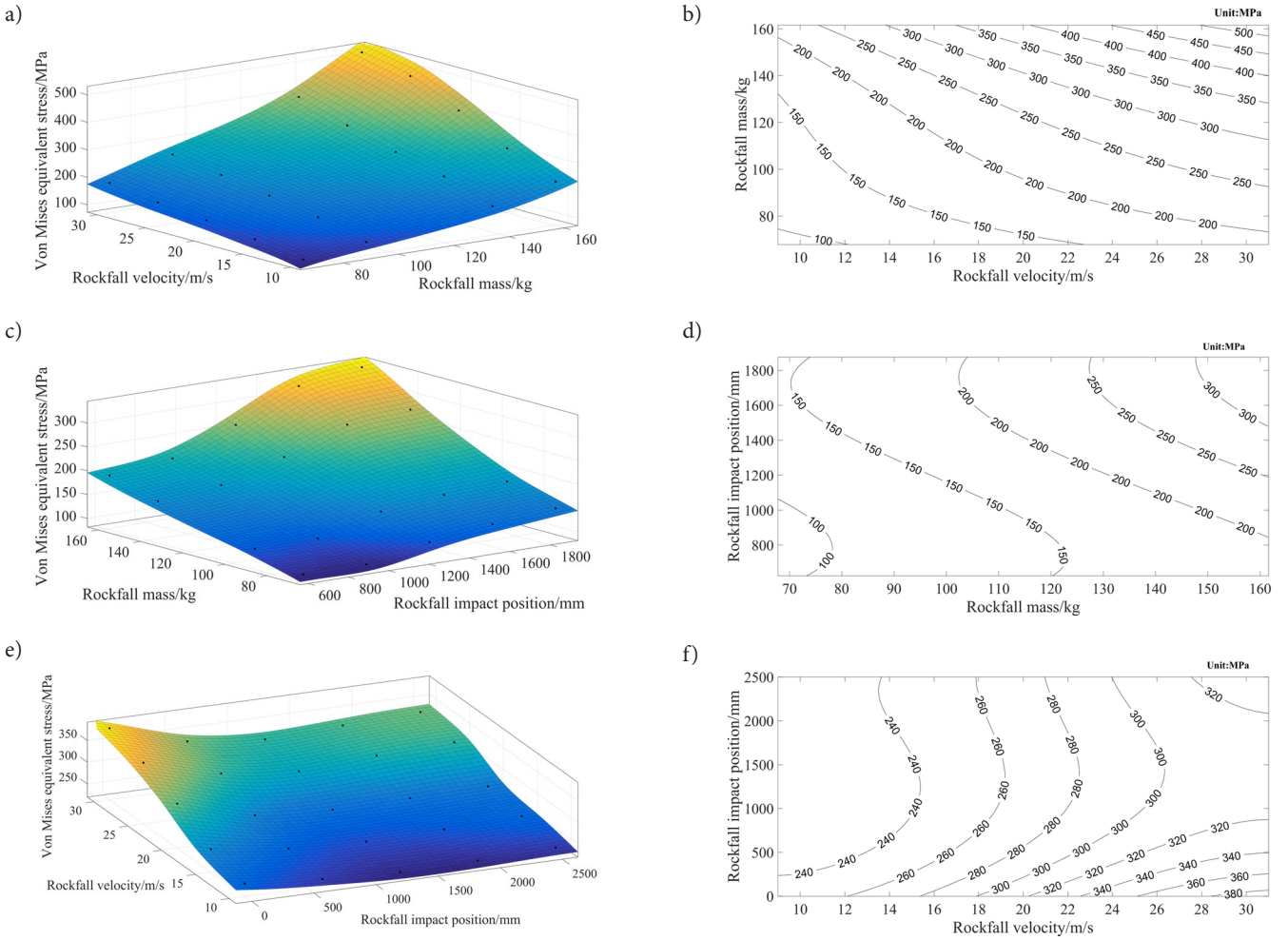

Fig. 12. Investigations of rockfall impact parameters on stress after the rockfall impact: a) stress vs. rockfall velocity and rockfall mass, b) contour map of Fig.12a), c) stress vs. rockfall mass and impact position, d) contour map of Fig.12c), e) stress vs. rockfall velocity and impact position, f) contour map of Fig.12e)

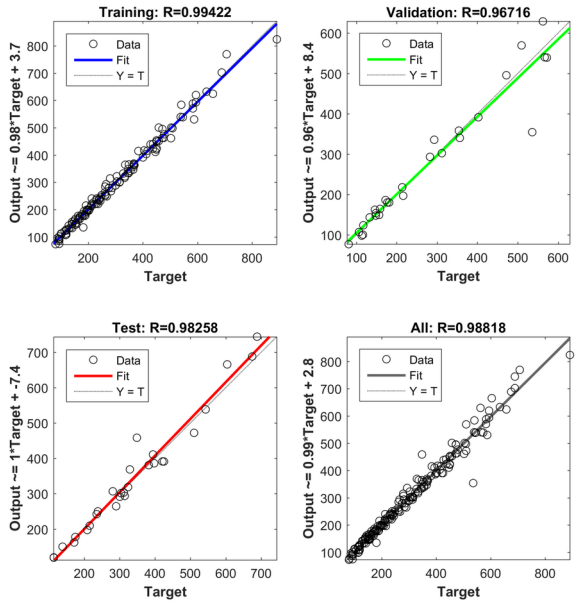

Fig. 13. R value corresponding to ANN model

soil again, the impact force on the ground is significantly reduced, and the kinetic energy after the rebound is far less than that for the first time. Thus, during the process of the rockfall impact on the buried pipeline, the rockfall's first impact has the most significant harm to the pipeline.

Here, the MCS is applied to evaluate the variation of the buried corroded pipeline's failure probability. The distributions for the pipeline's parameters are shown in Table 4 [10]. Combined with the expected failure LSF of corroded pipeline, we can obtain the buried corroded pipeline's reliability before the rockfall impact by using MCS.

According to the proposed ANN Model, the von Mises stress can be predicted for different rockfall parameters. Based on the time-varying reliability theory, the time-varying failure probability model of corroded pipeline is established by taking the yield strength of pipeline material as the structural resistance and the equivalent stress caused by loads as the additional load. After calculating the crossing rate, the pipeline failure probability after rockfall impact can be obtained by Eq. (31). Among them, the parameters of crossing rate can be determined by Eqs. (34)-(39). The changes of pipeline reliability after rockfall impact are shown in Figs. 14-16 respectively.

5.6. Sensitivity analysis

In this section, the sensitivity analysis of the rockfall impact velocity, mass, and impact position on pipeline's reliability is conducted. Generally, the greater the impact energy is, and the more prone the buried pipeline will fail. The selected numerical cases focus mainly on the extreme cases, and the rockfall's impact velocity is 30 m/s. The results for different rockfall masses are compared, as shown in Fig. 14.

Fig. 14 shows the impact analysis results of the rockfall mass on the pipeline's reliability. The rockfall's impact velocity is fixed at 30m/s. The pipeline's reliability under different rockfall masses are shown in Fig. 14(a). Obviously, with the increase of rockfall's mass, the pipeline's reliability decreases. The reason is that the increase of rockfall's

Table 4. Parameters of various pipeline distributions

Parameters	Mean value	Standard deviation	Distribution type
Diameter/mm	813.00	18.00	Normal
Wall thickness/mm	8.00	0.07	Normal
Yield strength/MPa	448.50	28.00	Normal
Tensile strength/MPa	535.00	36.00	Normal
Internal pressure/MPa	2.00	0.80	Normal
Initial corrosion depth/mm	4.00	0.15	Lognormal
Initial corrosion length/mm	400.00	2.00	Lognormal

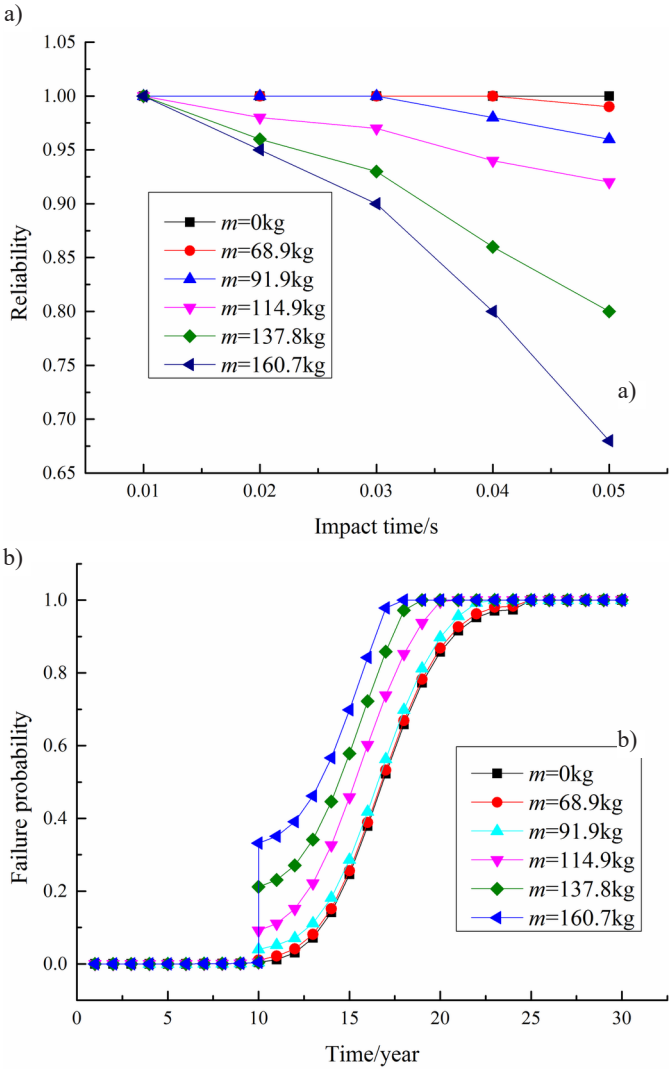

Fig. 14. The effect of different rockfall masses on pipeline's reliability: a) pipeline's reliability, b) pipeline's failure probability

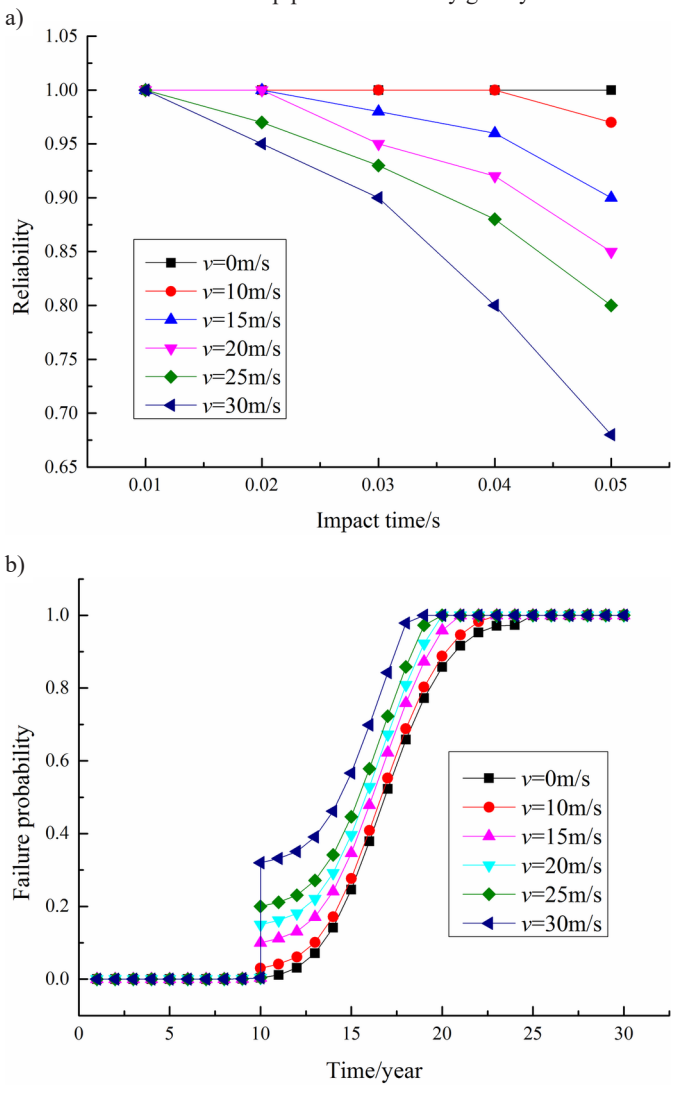

Fig. 15. The effect of different impact velocities on pipeline reliability: a) pipeline's reliability, b) pipeline's failure probability

mass will increase the impact's energy, thus increase the pipe's deformation and reduce its strength. Furthermore, with the increase of the rockfall's mass, the rockfall's energy impact to the soil is gradually enhanced, which will significantly reduce the pipeline's reliability. Fig. 14(b) shows the impact of rockfall's mass on the pipeline's reliability. The rockfall impact happens in the 10th year. And the curve of m=0 kg indicates that there is no rockfall impact as the reference line. It can be seen that the rockfall impact has great impact on the buried pipeline's reliability. Moreover, compared with no rockfall impact, there exists a sudden change in the 10th year. With the increase of the rockfall mass, the failure probability of the pipeline increases significantly.

Fig. 15 shows the results of the impact velocity on the pipeline's reliability, where the rockfall mass is 160.7kg. Fig. 15(a) shows the real-time change of pipeline's reliability under different impact speeds. When the velocity of the impact is small, the pipeline's reliability remains at a high level. As the impact velocity increases gradually from 10m/s to 30m/s, the reliability declines significantly. The reason is that with the increase of the impact velocity, the pipeline deformation and the local equivalent stress will increase, and it is closer to the critical yield strength. When the impact velocity reaches 30m/s, the pipeline's reliability will be far lower than the allowable reliability. Fig. 15(b) indicates that the impact velocity can affect the pipeline's reliability greatly.

Fig. 16 shows the results of the impact's position on pipeline's reliability. The impact's position is evaluated as the axial distance from the center of the corrosion defect. The variation of the pipeline's reliability with different impact positions is shown in Fig. 16(a). The results show that as the impact position increases from 0 mm and when it is smaller than the critical impact position (i.e. 1250 mm), the reliability will increase. However, when the impact position exceeds 1250 mm, the pipeline's reliability will decrease. Fig. 16(b) shows the curves of pipeline's failure probability when the rockfall impact

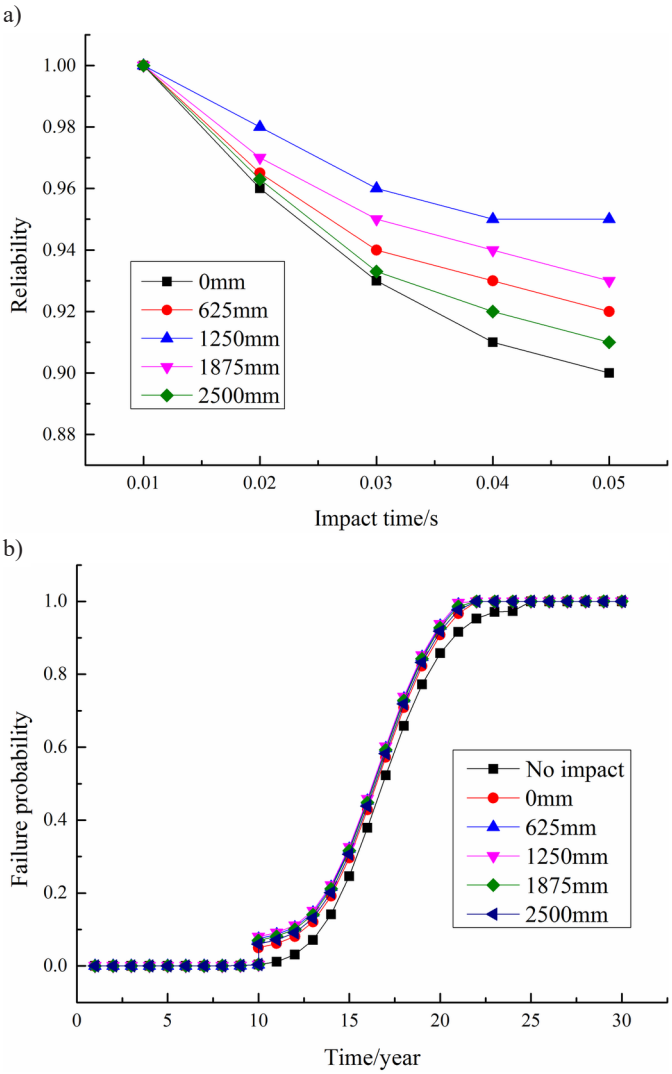

Fig. 16. The effect of impact's positions on the pipeline's reliability: a) pipeline's reliability, b) pipeline's failure probability

happens in the 10th year. It is found that under the rockfall impact, the pipeline's failure probability will increase instantaneously at the impact time, and it will result in the increase of the subsequent failure probability. However, compared with the impact mass and velocity, the impact's position has relatively small impact on the pipeline's reliability.

As a summary, the mass and velocity of the rockfall can significantly affect the pipeline's reliability. Therefore, to evaluate pipeline's reliability accurately, it is essential to take into account the effect of the rockfall's impact.

6. Conclusions

In this study, a novel approach is proposed to evaluate the effect of rockfall impact on the buried pipeline's reliability, where the finite element simulation and time-varying reliability theory are integrated. The finite elements model of pipeline-soil-rockfall is established by ABAQUS, and the pipeline's stress-strain results under the rockfall impact are analyzed. Moreover, the results are also verified with the results from theoretical mechanical modeling. It is found that the length and width of the corrosion defects have little influence on von Mises equivalent stress, and the depth of defects has a great influence. The rockfall's mass and velocity have relatively large effect on the pipeline's dynamic response and failure probability. While the variation of rockfall impact's axial distance from the corrosion defect has a relatively small effect on the pipeline's reliability. The proposed method can help to make decisions regarding the pipeline's integrity planning in engineering practice.

Actually, besides the rockfall impact, the buried pipeline's reliability is affected by various types of environmental factors. In this paper, the impacts of rockfall's velocity, mass and impact position on the pipeline's reliability are studied. In the future, other factors can be considered further, including internal pressure, buried depth, etc. Moreover, to better evaluate the pipeline's reliability, we can improve the accuracy of finite element simulation by establishing a pipe-soil geometric model more close to the actual working condition and improving the relevant soil parameters.

Acknowledgement

This work was supported by from the National Natural Science Foundation of China (NSFC) under grant No. 72001039 and 71671035; the Open Fund of Hunan Provincial Key Laboratory of Health Maintenance for Mechanical Equipment, China under No.201901; and the Open Fund of Jiangsu Wind Power Engineering Technology Center of China under ZK19-03-03.

References

1. Abyani M, Bahaari MR. A new approach for finite element based reliability evaluation of offshore corroded pipelines. International Journal of Pressure Vessels and Piping 2021; 193:104449, https://doi.org/10.1016/j.ijpvp.2021.104449
2. Aryai V, Baji H, Mahmoodian M, et al. Time-dependent finite element reliability assessment of cast-iron water pipes subjected to spatio-temporal correlated corrosion process. Reliability Engineering & System Safety 2020; 197:106802, https://doi.org/10.1016/j.ress.2020.106802.
3. Chekroun A, Kuniya T. Global threshold dynamics of an infection age-structured SIR epidemic model with diffusion under the Dirichlet boundary condition. Journal of Differential Equations 2020; 269: 117–148, https://doi.org/10.1016/j.jde.2020.04.046.
4. Davaripour F, Quinton BWT, Pike K. An assessment on a subsea pipeline subject to a diagonal trawl impact. Applied Ocean Research 2021; 110: 102575, https://doi.org/10.1016/j.apor.2021.102575.
5. Guillal A, Seghier MEAB, Nourddine A, et al. Probabilistic investigation on the reliability assessment of mid- and high-strength pipelines under corrosion and fracture conditions. Engineering Failure Analysis 2020; 118: 104891, https://doi.org/10.1016/j.engfailanal.2020.104891.
6. Han J, Naggar M, Zhao M, et al. Longitudinal response of buried pipeline under non-uniform seismic excitation from multi-point shaking table tests. Soil Dynamics and Earthquake Engineering 2021; 140(2):106440, https://doi.org/10.1016/j.soildyn.2020.106440.
7. Ismail S, Sadek S, Najjar SS, et al. Numerical finite element modelling of soil resistance against upheaval buckling of buried submarine pipelines. Applied Ocean Research 2021; 106(8):102478, https://doi.org/10.1016/j.apor.2020.102478.
8. Jiang FY, Dong S, Zhao YL, et al. Investigation on the deformation response of submarine pipelines subjected to impact loads by dropped objects. Ocean Engineering 2019; 194: 106638, https://doi.org/10.1016/j.oceaneng.2019.106638.
9. Kanjilal O, Papaioannou I, Straub D. Cross entropy-based importance sampling for first-passage probability estimation of randomly excited linear structures with parameter uncertainty. Structural Safety 2021; 91: 102090, https://doi.org/10.1016/j.strusafe.2021.102090
10. Karamitros DK, Bouckovalas GD, Kouretzis GP. Stress analysis of buried steel pipelines at strike-slip fault crossings. Soil Dynamics and Earthquake Engineering 2007; 27: 200–211, https://doi.org/10.1016/j.soildyn.2006.08.001.
11. Khusainov RB. Longitudinal deformation wave in a buried pipeline subject to viscoelastic interaction with soil. Soil Mechanics and Foundation Engineering 2020; 56: 420–426, https://doi.org/10.1007/s11204-020-09625-8.

12. Li J, Yan M, Yu J. Evaluation on gas supply reliability of urban gas pipeline network. Eksploatacja i Niezawodnosc - Maintenance and Reliability 2018, 20(3):471-477, http://doi.org/10.17531/ein.2018.3.17.
13. Li Y, Zhang Y, Kennedy D. Reliability analysis of subsea pipelines under spatially varying ground motions by using subset simulation. Reliability Engineering & System Safety 2018; 172: 74–83, https://doi.org/10.1016/j.ress.2017.12.006.
14. Liu AH, Chen K, Huang XF, et al. Corrosion failure probability analysis of buried gas pipelines based on subset simulation. Journal of Loss Prevention in the Process Industries 2019; 57: 25–33, https://doi.org/10.1016/j.jlp.2018.11.008.
15. Lotovskyi E, Teixeira AP, Soares CG. Availability analysis of an offshore oil and gas production system subjected to age-based preventive maintenance by Petri Nets. Eksploatacja i Niezawodnosc - Maintenance and Reliability 2020; 22(4):627-637, http://doi.org/10.17531/ein.2020.4.6.
16. Manolis GD, Stefanou G, Markou AA. Dynamic response of buried pipelines in randomly structured soil. Soil Dynamics and Earthquake Engineering 2020; 128:105873, https://doi.org/10.1016/j.soildyn.2019.105873.
17. Nahal M, Chateauneuf A, Sahraoui Y. Reliability analysis of irregular zones in pipelines under both effects of corrosion and residual stress. Engineering Failure Analysis 2019; 98:177-188, https://doi.org/10.1016/j.engfailanal.2019.01.081.
18. Pourhassan MR, Raissi S, Hafezalkotob A. A simulation approach on reliability assessment of complex system subject to stochastic degradation and random shock. Eksploatacja i Niezawodnosc - Maintenance and Reliability 2020; 22(2): 370-379, http://doi. org/10.17531/ein.2020.2.20.
19. Qin G, Cheng YF. Failure pressure prediction by defect assessment and finite element modelling on natural gas pipelines under cyclic loading. Journal of Natural Gas Science and Engineering 2020; 81:103445, https://doi.org/10.1016/j.jngse.2020.103445.
20. Sahraoui Y, Benamira M, Nahal M, et al. The effect of welded joint repair on a corroded pipeline reliability subjected to the hardness spatial variability and soil aggressiveness. Engineering Failure Analysis 2020; 118: 104854, https://doi.org/10.1016/j.engfailanal.2020.104854.
21. Shin MB, Park DS, Seo YK. Response of subsea pipelines to anchor impacts considering pipe–soil–rock interactions. International Journal of Impact Engineering 2020; 143:103590, https://doi.org/10.1016/j.ijimpeng.2020.103590.
22. Tian Y, Chai WS, Borgi S, et al. Assessment of submarine pipeline damages subjected to falling object impact considering the effect of seabed. Marine Structures 2021; 78: 102963, https://doi.org/10.1016/j.marstruc.2021.102963.
23. Wang WG, Wang YL, Zhang BH, et al. Failure prediction of buried pipe network with multiple failure modes and spatial randomness of corrosion. International Journal of Pressure Vessels and Piping 2021; 191: 104367, https://doi.org/10.1016/j.ijpvp.2021.104367.
24. Wang Y, Zhang P, Qin G. Non-probabilistic time-dependent reliability analysis for suspended pipeline with corrosion defects based on interval model. Process Safety and Environmental Protection 2019; 124: 290–298, https://doi.org/10.1016/j.psep.2019.02.028.
25. Wang Y, Zhang P, Qin G. Reliability assessment of pitting corrosion of pipeline under spatiotemporal earthquake including spatial-dependent corrosion growth. Process Safety and Environmental Protection 2021; 148: 166–178, https://doi.org/10.1016/j.psep.2020.10.005.
26. Xie MJ, Tian ZG. A review on pipeline integrity management utilizing in-line inspection data. Engineering Failure Analysis 2018; 92: 222–239, https://doi.org/10.1016/j.engfailanal.2018.05.010.
27. Xie MJ, Tian ZG. Risk-based pipeline re-assessment optimization considering corrosion defects. Sustainable Cities and Society 2018; 38: 746–757, https://doi.org/10.1016/j.scs.2018.01.021.
28. Xu X, He K, Su Y. Safety analysis of pipe–soil coordination deformation affected by mining subsidence. Geotechnical and Geological Engineering 2020; 38: 2187–2198, https://doi.org/10.1007/s10706-019-01156-w.
29. Yan YF, Shao B, Wang JJ, et al. A study on stress of buried oil and gas pipeline crossing a fault based on thin shell FEM model. Tunnelling and Underground Space Technology 2018; 81: 472–479, https://doi.org/10.1016/j.tust.2018.08.031.
30. Zelmati D, Bouledroua O, Ghelloudj O, et al. A probabilistic approach to estimate the remaining life and reliability of corroded pipelines. Journal of Natural Gas Science and Engineering 2021; 99:104387, https://doi.org/10.1016/j.jngse.2021.104387.
31. Zha SX, Wu Y, Jin PW. Reliability analysis of buried polyethylene pipeline subject to traffic loads. Advances in Mechanical Engineering 2019; 11(10): 168781401988378, https://doi.org/10.1177/1687814019883785.
32. Zhang DQ, Han X, Jiang C, et al. Time-dependent reliability analysis through response surface method. Journal of Mechanical Design 2017; 139: 041404, https://doi.org/10.1115/1.4035860.
33. Zhang J, Liang Z, Han CJ. Failure analysis and finite element simulation of above ground oil–gas pipeline impacted by rockfall. Journal of Failure Analysis and Prevention 2014; 14: 530–536, https://doi.org/10.1007/s11668-014-9847-x.
34. Zhang J, Liang Z, Feng D, et al. Response of the buried steel pipeline caused by perilous rock impact: Parametric study. Journal of Loss Prevention in the Process Industries 2016; 43: 385–396, https://doi.org/10.1016/j.jlp.2016.06.019.
35. Zhang J, Liang Z, Han CJ, et al. Buckling behaviour analysis of a buried steel pipeline in rock stratum impacted by a rockfall. Engineering Failure Analysis 2015; 58: 281–294, https://doi.org/10.1016/j.engfailanal.2015.09.009.
36. Zhang N, Jiang GJ, Wu DW, et al. Fatigue reliability analysis of the brake pads considering strength degradation. Eksploatacja i Niezawodnosc – Maintenance and Reliability 2020; 22 (4): 620–626, http://doi.org/10.17531/ein.2020.4.5.
37. Zhou S, Zhang J, You L, et al. Uncertainty propagation in structural reliability with implicit limit state functions under aleatory and epistemic uncertainties. Eksploatacja i Niezawodnosc – Maintenance and Reliability 2021; 23 (2): 231–241, http://doi.org/10.17531/ein.2021.2.3.